Configuration of the HERA Element

David DeBoer and Aaron Parsons

May 21, 2015

1 Introduction

The design of the HERA element is driven by advances in our understanding of how an interferometer's chromatic response interacts with foreground emission to produce systematics in power spectral measurements of the 21cm reionization signal.

2 Understanding Instrumental Chromaticity in the Context of the Wedge

For this discussion, we average the three-dimensional power spectrum $P(\mathbf{k})$ along a cylinder of $k_x^2 + k_y^2 = {k_\perp}^2$, where $\mathbf{k} \equiv (k_x, k_y, k_\|)$ is the three-dimensional wavevector, (k_x, k_y) are taken to be in the plane of the sky, and $k_\|$ is measured along the line-of-sight (spectral) direction. Recent work has shown that, for an interferometer whose analog bandpass and beam chromaticity are sufficiently smooth, systematics arising from foreground emission are isolated in the cylindrically averaged power spectrum $P(k_\perp, k_\|)$ within a wedge-shaped region described by [**????**]:

$$\begin{aligned} |k_\|| &\leq \frac{Y}{X\nu} k_\perp + YS \\ &\leq \frac{Y}{c} b + YS, \end{aligned} \tag{1}$$

where X, Y are cosmological scalars relating angular size and spectral frequency to comoving physical size, respectively, ν is spectral frequency, and $b = |\mathbf{b}|$ is the magnitude of the baseline vector for antennas in an interferometric pair, which substitutes for $k_\perp$ according to the relation $\mathbf{k}_\perp = X\nu\mathbf{b}/c$. As we will derive below, S is an additional additive offset related to the combined spectral smoothness of foregrounds and the antenna response.

As pointed out in **?**, the factor of b/c in the second line of equation (1) can be interpreted as the light-crossing time or maximum geometric signal delay, $\tau_{b,max}$ associated with an interferometric baseline. Particularly for per-baseline analyses such as those employed on PAPER [**????**], *signal delay* turns out to be a powerful basis for understanding the chromatic effects of interferometric observations. Signal delay arises as the Fourier dual to spectral frequency, according to the delay transformation of a visibility,

$$\tilde{V}_{\mathbf{b}}(\tau) = \int d\nu \; V_{\mathbf{b}}(\nu) e^{2\pi i \tau \nu}. \tag{2}$$

The measurement equation defines the visibility as

$$V_{\mathbf{b}}(\nu) = \int d\Omega \; A(\hat{s}, \nu) \; I(\hat{s}, \nu) e^{-2\pi i \frac{\mathbf{b}\cdot\hat{s}}{c}\nu}, \tag{3}$$

where A is the antenna response as a function of directon $\hat{s}$ and I is the sky intensity. We define the geometric signal delay in direction $\hat{s}$ as $\tau_{\mathbf{b},\hat{s}} \equiv \mathbf{b} \cdot \hat{s}/c$ in order to re-express the delay-transformed visibility as

$$
\begin{aligned}
\tilde{V}_{\mathbf{b}}(\tau) &= \iint d\nu \; d\Omega \; A(\hat{s},\nu) \; I(\hat{s},\nu) e^{-2\pi i \nu(\tau_{\mathbf{b},\hat{s}}-\tau)} \\
&= \int d\Omega \; \tilde{A}(\hat{s},\tau) * \tilde{I}(\hat{s},\tau) * \delta_D(\tau_{\mathbf{b},\hat{s}}-\tau),
\end{aligned} \tag{4}
$$

where δ_D is the Dirac delta function, '$\tilde{}$' signifies Fourier transformation along the frequency axis, and '$*$' denotes convolution.

Under the "delay approximation" [**?**], signal delay τ can be interpreted as a reasonable approximation to $k_\parallel$, giving us the following relationship between the delay-transformed visibility and the power spectrum:

$$
\tilde{V}_{\mathbf{b}}^2(\tau) \approx \left(\frac{2k_B}{\lambda^2}\right)^2 \frac{\Omega B}{X^2 Y} \widehat{P}(\mathbf{k}_\perp, k_\parallel), \tag{5}
$$

where k_B is Boltzmann's constant, λ is spectral wavelength, Ω is the angular area of the power-squared beam [**?**], and B is the effective bandwidth over which the delay transformation is performed.

We can now revisit the bound on systematics arising from the interaction of foreground emission and instrumental chromaticism given in equation (1). Let us assume for a moment that A and I are perfectly flat functions of frequency, so that $\tilde{A}$ and $\tilde{I}$ are delta functions centered at $\tau = 0$. In this case, the value of $\tilde{V}_{\mathbf{b}}(\tau)$ is determined by the integral over $\tilde{A}(\hat{s},0)\;\tilde{I}(\hat{s},0)$ in the sky directions that satisfy $\tau_{\mathbf{b},\hat{s}} = \tau$. For a given baseline $\mathbf{b} = \mathbf{k}_\perp / X\nu$, $\tau_{\mathbf{b},\hat{s}}$ is bounded by $\tau_{b,max} = b/c$, implying that for the case we have outlined, $\tilde{V}_{\mathbf{b}}(\tau)$ must be zero outside of a region $|\tau| \leq b/c$. Under the delay approximation, $k_\parallel \approx Y\tau$, so we can use equation (5) say that $P(k_\perp, k_\parallel)$ must be zero outside of the region specified in equation (1) for $S = 0$.

The inclusion of S in equation (1) accounts for precisely the terms we neglected above: the spectral structure in A and I, or more precisely, the delay-domain width of

$$
\langle \tilde{A} * \tilde{I} \rangle(\tau) \equiv \int d\Omega \; \tilde{A}(\hat{s},\tau) * \tilde{I}(\hat{s},\tau), \tag{6}
$$

where $\langle \ldots \rangle$ denotes the average over solid angle. In order to determine S quantitatively, however, we must clarify what is the relevant width in delay-domain. The purpose of equation (1) is to illustrate the boundary between the systematics-dominated and signal-dominated regimes. As such, it makes the most sense to determine width by the interval in delay domain outside of which $\langle \tilde{A} * \tilde{I} \rangle(\tau)$ is below the expected level of the 21cm reionization signal. Spectrally smooth ($\tau \approx 0$) foregrounds are approximately four to five times brighter that the expected reionization signal [], so a conservative definition of S requires

$$
\frac{|\langle \tilde{A} * \tilde{I} \rangle(\tau)|}{|\langle \tilde{I} \rangle(\tau = 0)|} < 10^{-6}. \tag{7}
$$

In words, we define S as the delay interval over which $\langle \tilde{A} * \tilde{I} \rangle$ falls off by -60 dB.

Given this framework, an obvious design goal for an interferometer aiming to measure the 21cm reionization signal is create antennas that can be close-packed to minimize b, and which yield an antenna response that minimizes S. However, as we will explore in more detail below, these aims must be balanced against cost.

2.1 Inherent Chromaticity of Foregrounds

Before we explore antenna design, however, it would be convenient to set an upper bound on the contribution of $\tilde{I}$ in equation (7). XXX this is turning out to be a bit tricky. Result is strongly dependent on windowing. Choosing a Blackman-Harris window and playing with power-law spectral indices of -1 and -2, getting a width for $\tilde{I}$ in range of 10 to 60 ns.

Suggest diminishing returns associated with pushing instrumental chromaticity much lower than 10 to 60 ns.

Also, as we push antennas closer together, galactic synchrotron emission (our dominant foreground) gets brighter as $C_\ell \propto \ell^{-3}$ []. Under the assumption that $k_\parallel$ is the dominant component of $\mathbf{k}$ (which holds for the short baselines used in PAPER and HERA), this implies that $|\langle \tilde{A} * \tilde{I} \rangle(\tau)|^2$ must decrease more rapidly than τ^{-3} for a reduction in baseline length to result in a reduction in foreground contamination at a given $k_\parallel$ scale. Hence, the combined chromaticity of the antenna beam and the galactic synchrotron foreground set an effective minimum baseline length, shorter than which foreground systematics no longer decrease, and could even potientially extend further in $|k_\parallel|$. This departure from the strictly linear relationship in equation (1) (which we will call the "ankle") for the shortest baselines is a telltale sign of the influence of diffuse synchrotron emission.

XXX If get analytic derivation of foreground profile in delay working, relate to that here. Figure XXX in **?** shows evidence of the departure equation (1) described above for baselines shorter than $\lesssim 10$ wavelengths. Although this empirical result includes a contribution from the PAPER antenna beam, the constant additive term that $\tilde{A}$ contributes (XXX maybe should capture in eq 1 that I could be baseline-dep) to the wedge boundary does not change the position of the ankle. Also worth noting is that, although an ankle appears around ~ 9 wavelengths, the extent of the wedge in $k_\parallel$ continues to decrease slowly toward even shorter baselines. This implies that, while there are diminishing returns in foreground systematics for using baseline shorter than ~ 18 m (9 wavelengths at 150 MHz), there does not appear to be a strong penalty for doing so either.

2.2 Setting a Specification for Antenna Chromaticity

So far, we have largely ignored the contribution of the antenna term in $\langle \tilde{A} * \tilde{I} \rangle(\tau)$. We now have a handle on the chromaticism introduced by the baseline term in equation (3) and an indication of when shorter baselines stop linearly reducing the occupancy of foreground systematics in $|k_\parallel|$. As we argued above, $b \lesssim 20$ m is an approximate threshold for when the chromaticity of the baseline term is no longer dominant. This suggests that foreground systematics are unlikely to drop below a width in delay domain corresponding to $b/c \sim 60$ ns ($|k_\parallel| \sim 0.03h$ Mpc^{-1} at 150 MHz).

Therefore, a reasonable specification for an interferometer targeting 21cm power spectrum measurements and working outside the wedge to avoid foregrounds might be to equally partition a chromaticity budget (i.e. delay-domain width) between the baseline term $\delta_D(\tau_{\mathbf{b},\hat{s}} - \tau)$, the inherent foreground term $\tilde{I}(\hat{s}, \tau)$, and the antenna term $\tilde{A}(\hat{s}, \tau)$. As described in equation (7), the relevant delay domain width is measured at the -60 dB point. Therefore, the specification we set for the chromaticity of the antenna is

$$\frac{|\langle \tilde{A} \rangle(\hat{s}, \tau = 60 \text{ ns})|}{|\tilde{\langle A \rangle}(\hat{s}, \tau = 0 \text{ ns})|} < 10^{-6}. \tag{8}$$

Here, we have separated the antenna and sky terms in $\langle \tilde{A} * \tilde{I} \rangle(\tau)$ in order to set a specification for the antenna term alone.

Under this specification, we assume the final chromaticity (wedge width) to be the sum of the individual widths of the $\tilde{A}$, $\tilde{I}$, and $\delta_D(\tau_{\mathbf{b},\hat{s}} - \tau)$ terms, for a total of 180 ns ($|k_\parallel| = 0.9h$ Mpc^{-1} at 150 MHz).

3 HERA Element Design

The delay-spectrum analysis technique employed for HERA requires that foreground systematics be tightly bounded within a wedge-shaped region in $(k_\perp, k_\parallel)$ space, such that contamination outside of this region falls below the expected level of the 21cm reionization signal. The supplied value from the analysis team is that reflections must be reduced by at least -60 dB at 60 ns. Another formulation is VSWR < 1.002 integrated over fluctuation scales of $\Delta\nu \leq 17$ MHz.

Assuming that HERA elements will have to deliver substantially more collecting area per feed than the current PAPER design, we adopted a parametrizable design based on a parabolic dish with a feed suspended over it. Thus, the diameter of the HERA dish is set by three factors:

1. meeting the chromaticity specification of -60 dB at 60 ns,
2. minimizing the impact of baseline-coupling systematics, and
3. minimizing cost for a fixed sensitivity

3.1 Focal Ratio

The diameter of the HERA antenna is set by three factors: (1) meeting the delay reflection specification of 60 dB at 60 ns, (2) lessening the impact of systematics, (3) lessening cost for a fixed sensitivity.

4 Delay

The delay-delayrate analysis technique employed for HERA requires that the region of phase space employed has contamination below the level of the signal. The supplied value from the analysis team is that reflections must be reduced by at least 60 dB at 60 ns. Another formulation is VSWR < 1.002 at frequencies below 15 MHz. The reflections between the feed and vertex is a chief contributor. The determine the delay scale a focal ratio must be used. A series of analytical models was run at several diameters using the calculated beam pattern of the PAPER feed. The results are shown in Figure 1. Note that they all peak at about a focal ratio of 0.32 (the solid lines with the x-axis divided by 10).

The dominant source of chromaticism within the antenna can be identified with internal signal reflections. Diffraction around dish edges and the evolving response of the feed also introduce chromaticism, but the scale of these frequency-dependent effects are expected to be significantly broader than the specified 16 MHz scale. In order to be problematic, signal reflections originating at the feed must re-enter the feed after a time delay of 60 ns before they are attenuated by -60 dB. Taking a geometric interpretation for an ideal paraboloid, off-axis emission from the feed is reflected out to the sky without re-entering the feed. Therefore, the dominant source of reflections is expected to arise between the feed and vertex. If reflections between the feed and vertex are dominant, the most important determinant of the timescale of reflections will be the feed height above the vertex. This implies that the focal ratio (the ratio of the focal height f to the diameter D) of paraboloid dish is one of the key aspects determining delay-spectrum performance.

Assuming a feed based on the PAPER design for a backplane without flaps, we computed analytical models at XXX MHz versus diameter over a 3.4–4.6 m range in focal height for an ideal parabolic dish. These models were used to determine the total efficiency of feed/reflector system, with efficiency η computed as the effective collecting area relative to the total geometric collecting area of a circular aperture of the indicated diameter. As shown in Figure 1, model efficiencies peak at $\eta \approx 0.73$ for focal ratios of $f/D \approx 0.32$, largely independent of the absolute scale of diameter.

4.1 Timescale and Amplitude of Feed-Vertex Reflections

Here, we adopt the focal ratio of $f/D = 0.32$ derived in the previous section in the context of maximizing efficiency. In doing so, we reduce the parametrization of our parabolic dish to a single degree of freedom: the diameter D. We may then explore how the timescale and amplitude of reflections between the feed and the vertex of the paraboloid scale with D.

Although the focal heights that we will discuss generally place the feed and dish within the five-wavelength threshold for treatment as a near-field system, we will nonetheless use a geometric (far-field) model as a tool for determining coarse scaling relationships. Geometrically, waves arriving at the feed from the sky absorbed and reflected in accordance with the impedance match between free space and the feed/balun system. The reflected wave is essentially re-emitted from the feed into the dish, and bulk of it is reflected back to the sky. However, as discussed previously, emission

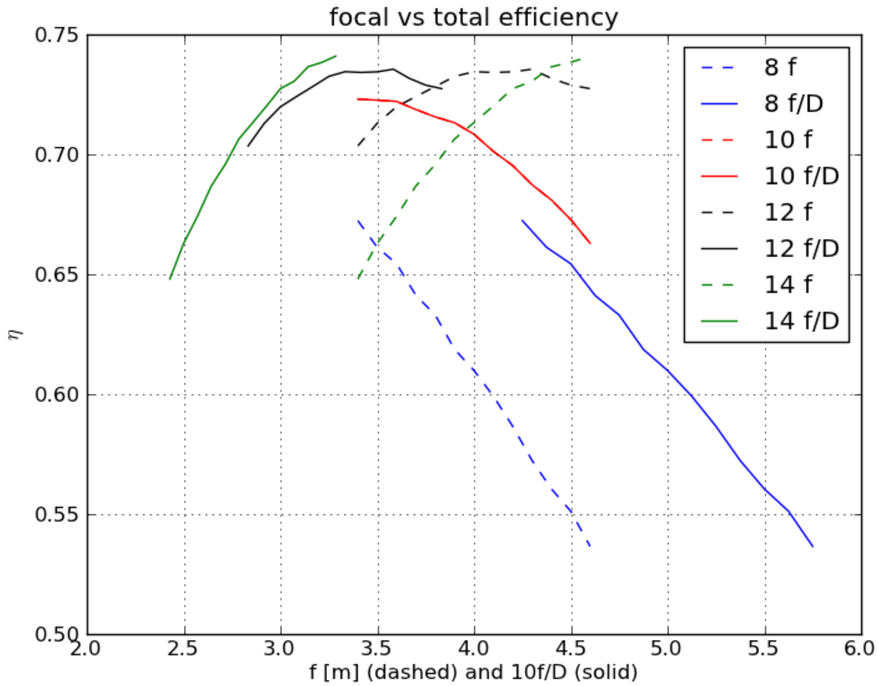

Figure 1: The model efficiency of a PAPER feed suspended over an ideal parabolic dish. The dashed curves indicate the efficiencies over a 3.4–4.6 m range in focal height f for the dish diameters D indicated in the legend. The solid curves extrapolate the model efficiencies of the corresponding dashed curves to a $D = 10$ m dish (note the red dashed and solid curves are identical). The approximate agreement of the solid curves indicates that to first order, efficiency is a function of the focal ratio f/D. The absolute scaling of η with D appears as a second-order (few percent) increase in efficiency. Hence, peak efficiencies of order $\eta \approx 0.73$ are expected for focal ratios of $f/D \approx 0.32$.

toward the the vertex of the parabola may be reflected back toward the feed, whereupon the absorption/reflection process repeats with an attenuated amplitude.

We begin by computing the round-trip light-propagation times between the vertex and feed. Figure 2 shows the resulting signal delay for reflections spanning 1, 2 and 3 round trips. To interpret the results, let us explore different cases. If we assume that after two reflections, the reflected signal has been attenuated below the -60 dB threshold in the specification, then the first reflection (which is above the threshold) must have a timescale shorter than 60 ns. Following the curve for 1 round-trip reflection, we see that a 28-m dish (with a focal height of ~ 9 m) is the maximum size that would meet specification. If, on the other hand, a -60 dB attenuation is only achieved on the third reflection, then the curve for 2 round trips suggests a maximum diameter of 14 m. Similarly, requiring the attenuation associated with one more reflection moves the maximum diameter down to 9.4 m.

Finally, we may ask, given the number of reflections that fall inside of 60 ns, what is the attenuation per reflection Γ that puts the signal level below -60 dB after 60 ns? Here, Γ includes all loss factors, including the reflection coefficient associated with the impedance match of the feed, path loss, etc. Illustrated in Figure 3 is the total attenuation of a signal arriving at timescales <60 ns, given as a function of Γ for the indicated number of reflections falling inside 60 ns.

Combining the results in Figures 2 and 3, we can see that dishes with $D < 9.4$ m must have $\Gamma < -15$ dB, dishes where $9.4 \text{ m} < D < 14$ m require $\Gamma < -20$ dB, and those with diameters $14 \text{ m} < D < 28$ m need $\Gamma < -30$ dB.

It is worth noting that imperfect impedance matches in the feed as a function of frequency generally place the reflection coefficient of the feed itself in the range of -5 to -15 dB. We must rely

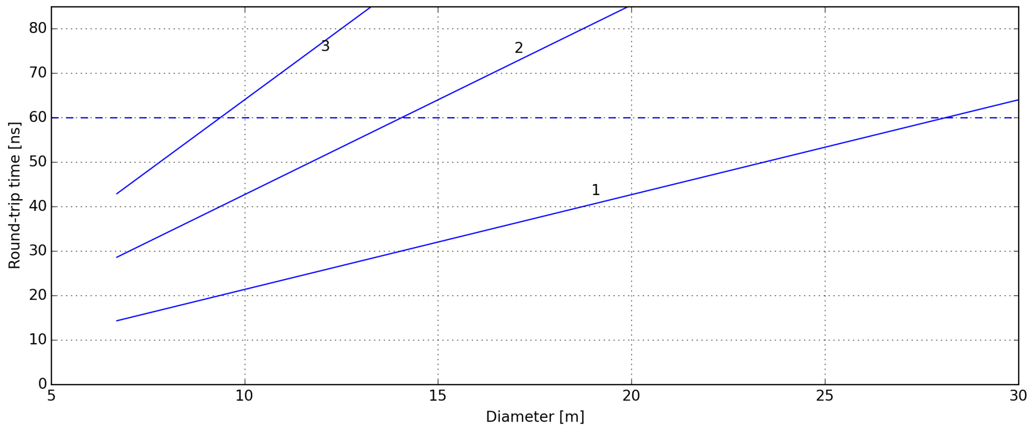

Figure 2: Round-trip propagation times between feed and vertex for $f/D = 0.32$, shown for 1, 2, and 3 reflections. The 60-ns timescale appearing in the specification is indicated with a dashed line.

on directing reflected waves away from the feed to achieve the total attenuation per reflection that is required. Geometrically, we can estimate that for a parabolic reflector that reflects emission from the feed straight upward, a wave must intersect the paraboloid at a distance of half a wavelength off axis to avoid passing close enough to the feed to be re-absorbed. Assuming $\lambda = 2$ m, this angle is

$$\phi \approx \tan^{-1}\frac{1}{f}. \tag{9}$$

For a 14-m dish with a focal ratio of $f/D = 0.32$ ($f \approx 4.5$ m), $\alpha \approx 13°$. This gives a solid angle of 0.15 sr into which the feed must emit in order to receive the reflection. We can calculate the power emitted into this region numerically given a model of the feed response, but coarsely, for a feed emitting uniformly into 2π sr, the power emitted into this region represents -16 dB of the total reflected power.

Thus, it seems likely that $\Gamma \sim -20$ dB is achievable, while $\Gamma \sim -30$ dB would require careful tuning of the feed and dish.

INCLUDE PLOT OF RELECTOMETRY TESTS

5 Systematics

As described above, minimizing internal reflections that introduce signal delays is the primary design requirement of the HERA dish. A secondary consideration is the reduction of cross-coupling between the feeds of adjacent dishes. Since the focus of the parabolic dish lies above the rim, feeds potentially have a direct line of sight to one another. Noise and signal reflections emanating from one feed and coupling into another can introduce spurious correlations that show up, to first order, as a static (zero fringe rate) additive phase term with significant spectral structure.

Although current PAPER analysis removes such static correlations via fringe-rate filtering, this approach limits observing to regions away from the celestial poles, and significantly reduces the number of independent sky samples obtained with a given baseline. Although this approach may remain an imporant tool for dealing with feed cross-coupling, it would be nice to limit its necessity. One obvious way to do this is to shield feeds from one another.

To achieve this, the HERA dish design incorporates mesh screens at the boundaries of dishes that rise high enough to shield feeds from one another. In the limit of geometric optics, these screens perfectly isolate feeds from one another, but risk introducing a new internal reflection pathway. To avoid reflecting signals back into the feed, screens need to be tilted such that a ray originating from the feed and arriving at the screen are reflected upward far enough that they miss the feed

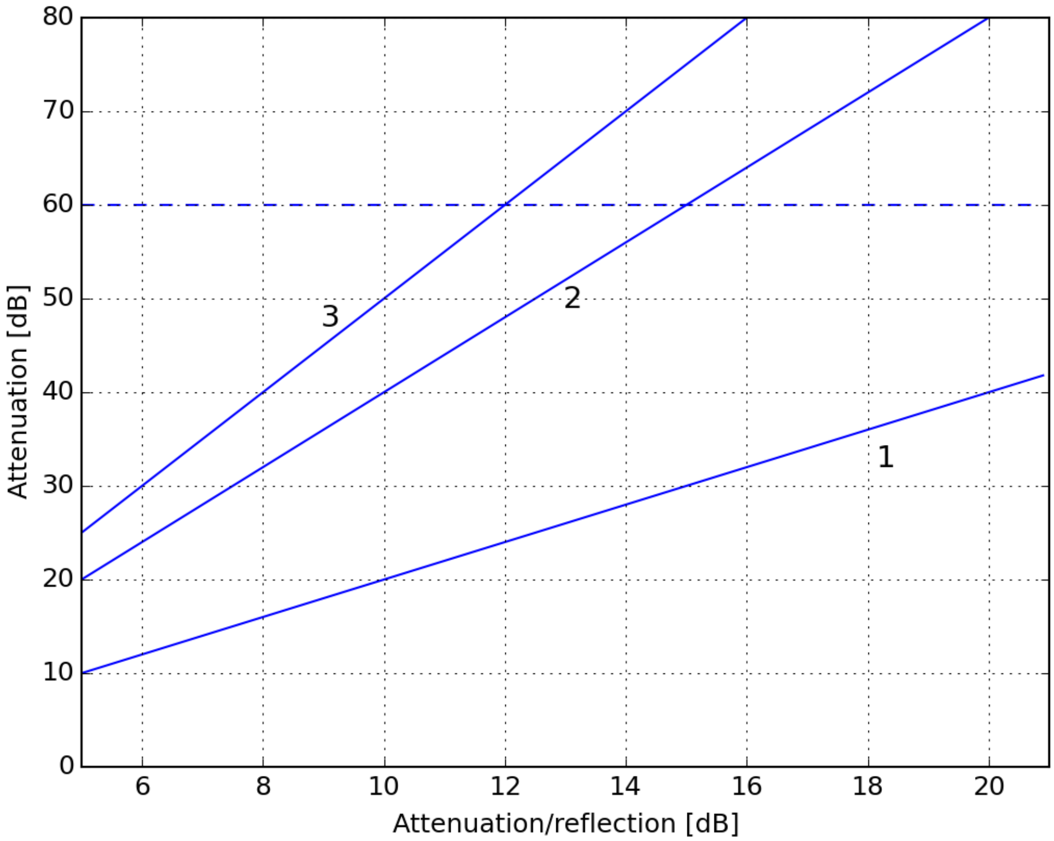

Figure 3: XXX curve 2 is right, but others are wrong. Switch signs of X and Y axes. Overall attenuation for 1, 2 and 3 trips.

by a wavelength. For a dish with a radius of $\sim$ 7 m and an observing wavelength of $\sim$2 m, this requires a tilt angle α given by $\tan\alpha = 1/7$. Thus, in the geometric limit, shielding screens must be approximately 8 degrees off of vertical.

In practice, we will not the geometric optical limit, and the above specification can only be a coarse rule of thumb. Most notably, the top edge of the screen will introduce diffraction that degrates feed-feed isolation. Scalloping or rolling the edges of screens may help reduce diffraction, but these ideas will need to be tested in the field to show their efficacy.

Pending field testing, HERA dishes are designed to include screens that rise $\sim$ 2 m from the rim ($\sim$0.75 m above the feeds), supported by the same large wooden poles that are used to suspend the feed. The bottom of these screens are held at a distance of 30 cm inward relative to the top, for a tilt of 8.5 degrees from vertical.

6 Sensitivity

The equation for sensitivity has been described in previous works [REFS] and depends on many parameters related to the instrumentation, the configuration, the location, the observing strategy, etc. A useful form for the proposed compact configuration is Eq 27 in [?] and reproduced here:

$$\Delta_N^2(k) \approx 60 \left[\frac{k}{0.1h\mathrm{Mpc}^{-1}}\right]^{\frac{5}{2}} \left[\frac{6\mathrm{MHz}}{B}\right]^{\frac{1}{2}} \left[\frac{1}{\Delta \ln k}\right]^{\frac{1}{2}} \times \left[\frac{\Omega}{0.76\mathrm{sr}}\right] \left[\frac{T_{\mathrm{sys}}}{500\mathrm{K}}\right]^2 \left[\frac{6\mathrm{hrs}}{t_{\mathrm{per\_day}}}\right]^{\frac{1}{2}} \times \left[\frac{120\mathrm{days}}{t_{\mathrm{cam}}}\right] \left[\frac{32}{N_a}\right] \left[\frac{10^4 f_o}{f}\right] \mathrm{mK}^2 \tag{10}$$

where k is the magnitude of the k-mode, B is the bandwidth, $\Delta \ln k$ is the log of the binsize, Ω is the field-of-view, T_{sys} is the system temperature, $t_{\mathrm{per\_day}}$ is the number of hours observed per day, t_{cam} is the number of days observed, N_a is the number of antennas, and f_o/f is the configuration metric for a redundant array as defined in [?].

Note that $\Delta_N^2(k)$ is the standard radiometric sensitivity equation, scaled by the volume in k-space, normalized by the power spectrum Fourier coefficient, and reduced by the number of independent samples in a given k-mode bin, which may have both coherent and incoherent application.

Pulling out terms relating to diameter (D_a) and number, we can write Eq. 10 as

$$\Delta_N^2(k) \propto \frac{\Omega(f_o/f)}{N_a\sqrt{t_{\mathrm{per\_day}}}} \propto \frac{(1/D_a^2)(1/\sqrt{N_a})}{N_a\sqrt{D_a}} = D_a^{-\frac{5}{2}} N_a^{-\frac{3}{2}} \tag{11}$$

where the dependencies on diameter and number have been substituted in, noting that the expressions for f_o/f and $t_{\mathrm{per_day}}$were derived in Parsons et al where the baselines for the close-packed array are multiples of the diameter.

Letting the reduced sensitivity be $C = D_a^{-\frac{5}{2}} N_a^{-\frac{3}{2}}$ and scaling for canonical values of $D_a = 14$ m, $N_a = 331$ m, the needed number of antennas as a function of diameter (shown in Fig 4) is

$$N_a = 26918 D_a^{-\frac{5}{3}} \tag{12}$$

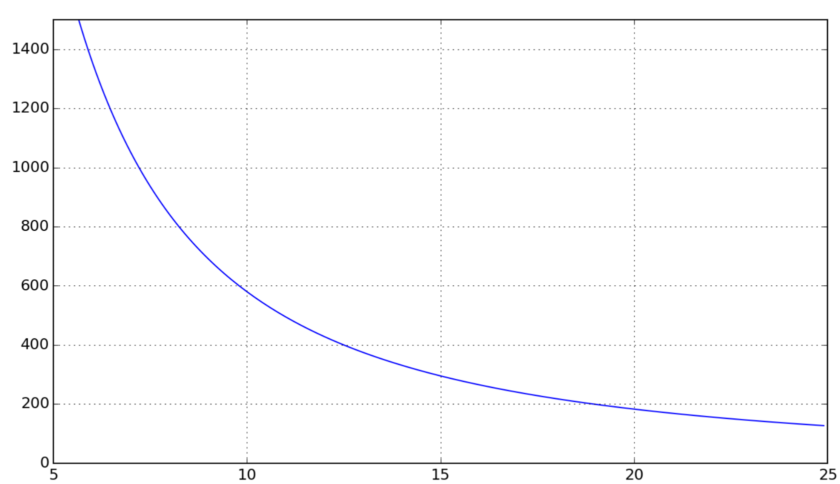

Figure 4: Number of antennas at fixed sensitivity with reference of 331 14-m antennas

The sensitivity specification is to maximize performance per cost, which determines the element diameter (D_a) and the number of elements (N_a) subject to the constraints above. One therefore needs a model of cost and performance as a function of D_a and N_a. Given a fairly mature element and system design, a bottoms-up costing appropriate for element diameters from about 6-m to 30-m has been done for hex-numbers corresponding to element counts from 91 to 1141. The costs here are only those associated with delivering the array to that scope on-site, so excluding development and science. The results are shown in Fig. 5. At diameters greater than about 12-m the cost function is relatively flat.

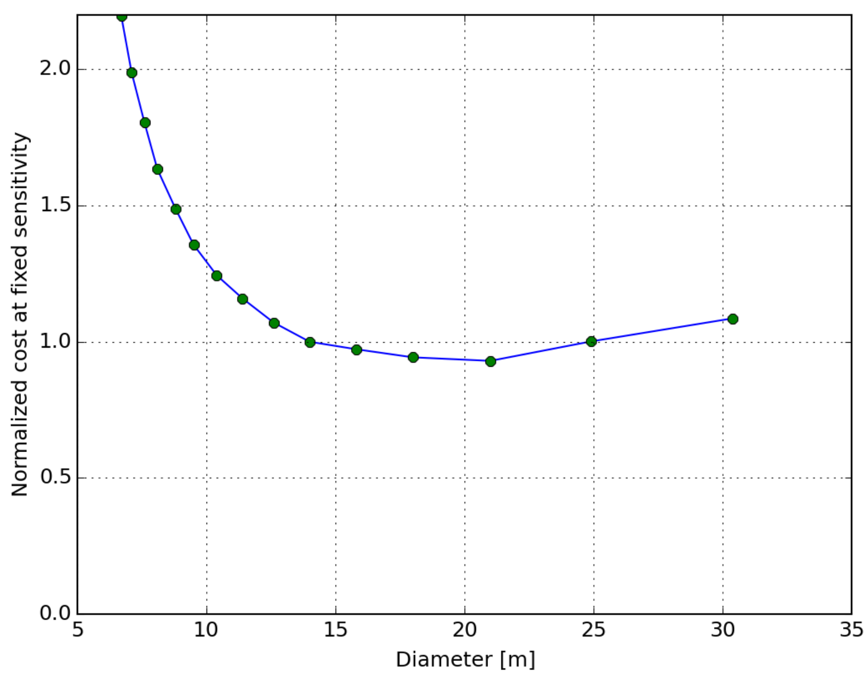

Figure 5: Normalized cost at fixed sensitivity with reference of 331 14-m antennas

References